

Splitting rates in QCD plasmas from a non-perturbative determination of the momentum broadening kernel $C(q_\perp)$

Sören Schlichting¹ and Ismail Soudi^{1,2}

¹*Fakultät für Physik, Universität Bielefeld
D-33615 Bielefeld, Germany.*

²*Department of Physics and Astronomy, Wayne State University
Detroit, MI 48201.*

(Dated: November 30, 2021)

We exploit a recent non-perturbative determination of the momentum broadening kernel $C(b_\perp)$ in impact parameter space [1], to determine the momentum space broadening kernel $C(q_\perp)$ in high-temperature QCD plasmas. We show how to use the non-perturbatively determined kernel $C(q_\perp)$ to compute the medium-induced splitting rates in a QCD plasma of finite size. We compare the resulting in-medium splitting rates to the results obtained with leading-order and next-to-leading order perturbative determinations of $C(q_\perp)$, as well as with various approximations of the splitting employed in the literature. Generally, we find that the differences in the splitting rates due to the momentum broadening kernel are larger than the errors associated with approximations of the splitting rate.

I. INTRODUCTION

One of the clearest signals for the formation of a Quark Gluon Plasma (QGP) in heavy ion collisions is the suppression of the yields of highly energetic particles. When highly energetic partons or jets traverse the medium, they interact with the constituents of the QGP leading to a loss of energy, commonly referred to as jet quenching [2]. While for highly energetic partons only a small fraction of the energy is lost due to elastic interactions with the medium, the interactions of hard partons with the medium constituents also induce additional “medium-induced” radiation [3–5], which provides the dominant energy loss mechanism for highly energetic particles. Studies of medium-induced radiation in QCD plasmas date back to the early determinations of the Landau-Pomeranchuk-Migdal effect [6, 7] in QCD [5, 8–10], and include determinations of the radiation rate in QCD plasmas of infinite [11] and finite spatial extent [12, 13]. Beyond the development of different theoretical formalism to determine the in-medium splitting rates [3–5, 8–10, 13–20], there have also been ongoing efforts to construct suitable approximations of the medium-induced splitting rates in various different limits [15, 16, 21–25].

In all the different formalisms to obtain splittings rates, the interaction of hard partons with the medium are described using the rate of transverse momentum broadening

$$C(q_\perp) \equiv (2\pi)^2 \frac{d\Gamma}{d^2q_\perp}, \quad (1)$$

which defines the rate to exchange transverse momentum q_\perp with the QCD medium. While perturbative broadening kernels have been used to successfully predict observables (see e.g. [26, 27] for recent reviews) it is known that due to the infrared (IR) problem, the perturbative expansion breaks down in the IR regime even at small

coupling [28]. Nevertheless, effective field theories coupled with lattice calculations can be used to evade the IR problem [29]. Specifically, for the momentum broadening kernel $C(q_\perp)$, one can define the zero-subtracted Fourier transform

$$C(b_\perp) \equiv \int \frac{d^2q_\perp}{(2\pi)^2} (1 - e^{iq_\perp \cdot b_\perp}) C(q_\perp). \quad (2)$$

which can be defined non-perturbatively in terms of certain light-like Wilson loops [30]. For temperatures well above the critical temperature T_c these light-like Wilson loops can be recast in the dimensionally reduced long-distance effective theory for QCD, 3D Electrostatic QCD (EQCD) [31]. In an earlier study [1] we showed how the short distance behavior of the broadening kernel $C_{\text{EQCD}}(b_\perp)$ determined from non-perturbative lattice simulations of EQCD [32–35], can be matched to obtain a non-perturbative determination of $C_{\text{QCD}}(b_\perp)$ in QCD at all scales. In this study the broadening kernel was computed in impact parameter (b_\perp) space, which is favorable for the calculation of medium-induced radiation in an infinite medium [36]. However, in order to extend the framework to a QCD medium of finite size, it is highly favorable to work in momentum (q_\perp) space [12].

Central objective of this paper is to employ the non-perturbative determination of $C_{\text{QCD}}(b_\perp)$ in [1], to determine the medium-induced radiation rates in the physically relevant situation of a finite medium. First, we Fourier transform the non-perturbative kernel to momentum space in Sec. II. Subsequently in Sec. III, we recapitulate the formalism of [12] to obtain the splitting rates in a finite medium and introduce the opacity expansion [16, 37] together with an expansion around the multiple soft scattering limit [22–24] and a resummed opacity expansion method [25]. Numerical results for the splitting rates are presented in Sec. IV, where we compare our calculations with the results obtained using leading order (LO) and next-to-leading order (NLO) perturbative determinations of the broadening kernels, and investigate

	$\left.\frac{C(b_\perp)}{g^2}\right _{250 \text{ MeV}}^{N_f=3}$	$\left.\frac{C(b_\perp)}{g^2}\right _{500 \text{ MeV}}^{N_f=3}$
g^2	3.725027	2.763516
$\hat{q}_0/g^6 T^3$	0.1465(78)	0.185(10)
ξ	0.1780	0.1702
$\sigma_{\text{EQCD}}/g^4 T^2$	0.2836(10)	0.2867(10)

TABLE I. Various constants that determine the limiting behavior of the non-perturbative momentum broadening kernel. Numerical values are reproduced from [1, 35].

the quality of various approximations. We conclude with a summary of our important findings in Sec. V.

II. NON-PERTURBATIVE BROADENING KERNEL

Building on earlier works that established the procedure [32–34], non-perturbative contributions to the momentum broadening kernel were extracted from an EQCD lattice calculation in [38]. However, since EQCD is an IR effective theory of QCD, the EQCD broadening kernel from [38] is only valid in the IR regime. In [1] we demonstrated how one can perform a matching to the QCD broadening kernel in UV regime to obtain a broadening kernel valid over the entire range of momenta/impact parameters [1]. By following the arguments [1, 39], the non-perturbative broadening kernel is determined as

$$C_{\text{QCD}}(b_\perp) \approx \left(C_{\text{QCD}}^{\text{pert}}(b_\perp) - C_{\text{subtr}}^{\text{pert}}(b_\perp) \right) + C_{\text{EQCD}}^{\text{latt}}(b_\perp), \quad (3)$$

where $C_{\text{QCD}}^{\text{pert}}(b_\perp)$ is the UV limit of the QCD kernel, which is known analytically in momentum space [31, 40]

$$C_{\text{QCD}}^{\text{pert}}(q_\perp) = \frac{g^4 C_R}{q_\perp^4} \int \frac{d^3 p}{(2\pi)^3} \frac{p - p_z}{p} [2C_A n_B(p) (1+n_B(p')) + 4 N_f T_f n_F(p) (1-n_F(p'))], \quad (4)$$

and the subtraction term $C_{\text{subtr}}^{\text{pert}}(q_\perp)$ is given by [39]

$$C_{\text{subtr}}^{\text{pert}}(q_\perp) = \frac{C_R g^2 T m_D^2}{q_\perp^4} - \frac{C_R C_A g^4 T^2}{16 q_\perp^3}, \quad (5)$$

where, as discussed in detail in [1], the first term cancels against the (unphysical) IR limit of $C_{\text{QCD}}^{\text{pert}}(q_\perp)$, while the second term cancels out the (unphysical) UV behavior of the EQCD kernel.

A. Broadening kernel in impact parameter space

Before we proceed to Fourier transform the resulting kernel to momentum space, we briefly recall the limiting behaviors of the kernel in impact parameter space.

At long-distances the Wilson loop follows an area-law behavior [41] with asymptotic corrections which are important for smoothening the transition to the numerical data values

$$\frac{C_{\text{QCD}}(b_\perp)}{g^2 T} \xrightarrow{b_\perp \gg 1/g^2 T} A + \frac{\sigma_{\text{EQCD}}}{g^4 T^2} g^2 T b_\perp + \frac{g^2 C_R}{\pi} \left[\frac{m_D^2}{4g^2 T^2} \left(\frac{1}{6} - \frac{1}{\pi^2} \right) + \frac{C_A}{8\pi^2} \right] \log(g^2 T b_\perp). \quad (6)$$

Here σ_{EQCD} is the string tension of EQCD [42] and A is a constant fitted to the EQCD lattice data [1].

Conversely, at short-distances, the broadening kernel follows a similar behavior to the leading order QCD behavior

$$\frac{C_{\text{QCD}}(b_\perp)}{g^2 T} \xrightarrow{b_\perp \ll 1/m_D} \frac{1}{4} \frac{\hat{q}_0}{g^4 T^3} (g T b_\perp)^2 - \frac{C_R \mathcal{N}}{8\pi} (g T b_\perp)^2 \log(g^2 T b_\perp), \quad (7)$$

where $\mathcal{N} = \frac{\zeta(3)}{\zeta(2)} \left(1 + \frac{N_f}{4} \right)$ and we provide the numerically extracted value of \hat{q}_0 in Tab. I which is reproduced from [1] for the sake of completeness of the presentation.

B. Broadening kernel in momentum space

We now proceed to perform the Fourier transform of the non-perturbative broadening kernel [1] back to momentum space. In principle, the inverse Fourier transform is standard and should be straightforward to compute. However, due to the sparseness of the data points, the divergent behavior of the kernel at large impact parameter and the highly oscillatory nature of the integrals involved, performing the numerical integral is actually rather challenging. To avoid these difficulties, we found that it is best to Fourier transform the coordinate space derivative $\frac{dC(b_\perp)}{db_\perp}$ of the momentum broadening kernel. Using Eq. (2), one can write

$$\frac{dC(b_\perp)}{db_\perp} = \int \frac{d^2 q_\perp}{(2\pi)^2} e^{-i q_\perp \cdot b_\perp} \left[\frac{i q_\perp \cdot b_\perp}{b_\perp} C(q_\perp) \right]. \quad (8)$$

Exploiting the fact that $C(q_\perp)$ does not depend on the direction $\mathbf{b}_\perp/|b_\perp|$ then leads to the following Hankel transform,

$$\frac{dC(b_\perp)}{db_\perp} = \int_0^\infty \frac{dq_\perp}{(2\pi)} q_\perp J_1(b_\perp q_\perp) [q_\perp C(q_\perp)], \quad (9)$$

where $J_1(x)$ is the Bessel function of the first kind of order 1. By use of the inverse Hankel transform, one then obtains the broadening kernel in momentum space as

$$C(q_\perp) = \frac{2\pi}{q_\perp} \int_0^\infty db_\perp b_\perp J_1(b_\perp q_\perp) \frac{dC(b_\perp)}{db_\perp}. \quad (10)$$

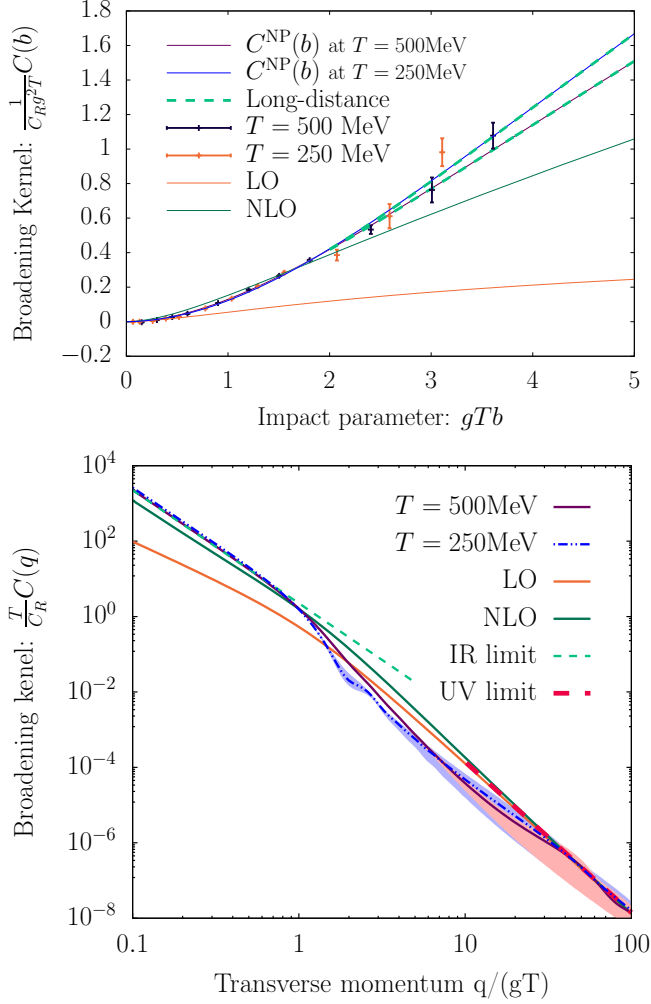


FIG. 1. (top) Non-perturbative elastic broadening kernel $C_{\text{QCD}}(\mathbf{b}_\perp)$ in impact parameter space. Data points for two different temperatures $T = 250, 500 \text{ MeV}$ are shown alongside the interpolating splines. We also compare to the short-distance limit in Eq. (7) and the long-distance limit in Eq. (6). (from [1]). (bottom) Elastic broadening kernel $C_{\text{QCD}}(\mathbf{q}_\perp)$ in momentum space for $T = 250, 500 \text{ MeV}$. Blue and purple bands represent uncertainties of the spline interpolation for 250 MeV and 500 MeV respectively. We also compare the kernel to leading-order (LO) and next-to-leading order (NLO) determinations, as well as to the UV limit in Eq. (17) and the IR limit in Eq. (16).

While the integral in Eq. (10) is still highly oscillatory, it can be computed numerically as long as the integrand is sufficiently well behaved at the integration boundaries. In order to ensure numerical convergence, we therefore subtract the leading asymptotic behavior at large distances

$$\frac{dC^{\text{IR}}(\mathbf{b}_\perp)}{db_\perp} = \frac{\sigma_{\text{EQCD}}}{g^4 T^2} g^4 T. \quad (11)$$

and only perform a numerical Hankel transform of the remainder

$$\frac{d}{db_\perp} \Delta C_{\text{QCD}}(\mathbf{b}_\perp) = \frac{dC_{\text{QCD}}(\mathbf{b}_\perp)}{db_\perp} - \frac{dC_{\text{QCD}}^{\text{IR}}(\mathbf{b}_\perp)}{db_\perp}, \quad (12)$$

which by construction vanishes for large impact parameters. By numerically performing the Hankel transform

$$\Delta C_{\text{QCD}}(q_\perp) = \frac{2\pi}{q_\perp} \int_0^\infty db_\perp b_\perp J_1(b_\perp q_\perp) \frac{d}{db_\perp} \Delta C_{\text{QCD}}(b_\perp), \quad (13)$$

and supplying it with the analytic result for the Hankel transform of $C^{\text{IR}}(\mathbf{b}_\perp)$, given by

$$C_{\text{QCD}}^{\text{IR}}(q_\perp) = \frac{2\pi}{q_\perp^3} \frac{\sigma_{\text{EQCD}}}{g^2 T}. \quad (14)$$

we obtain the full momentum broadening kernel as

$$C_{\text{QCD}}(q_\perp) = \Delta C_{\text{QCD}}(q_\perp) + C_{\text{QCD}}^{\text{IR}}(q_\perp), \quad (15)$$

We note that, due to the fact that the Bessel function is highly oscillatory for large momenta q_\perp , sufficient care should be taken in performing the integral, and we describe the procedure we employ in Appendix. A.

Next, in order to construct the momentum broadening kernel $C(q_\perp)$ at all scales we proceed to transform the limiting behaviors of the kernel, which can be used to extrapolate the results beyond the tabulated range of q_\perp values. In the deep infrared regime, the momentum broadening kernel is determined by the string tension, where as shown in Appendix. A, one finds

$$C_{\text{QCD}}(q_\perp) \xrightarrow{q_\perp \ll g^2 T} 2\pi \frac{\sigma_{\text{EQCD}}}{q_\perp^3} \quad (16)$$

In the UV limit the momentum broadening kernel follows the same behavior as the perturbative QCD kernel in Eq. (4), and one obtains [40]

$$C_{\text{QCD}}(q_\perp) \xrightarrow{q_\perp \gg m_D} \frac{C_R g^4 T^3 \mathcal{N}}{q_\perp^4}. \quad (17)$$

C. Perturbative kernel in EQCD

Before we present results for the non-perturbative determination of $C(q_\perp)$, we briefly recall the results of perturbative calculations, following [1, 39], which we will use as a reference for comparison. At leading order (LO) $\mathcal{O}(g^4)$, the QCD collisional broadening kernel can be expressed in momentum space [40] as

$$C_{\text{QCD}}^{\text{LO}}(q_\perp) = \frac{g^4 C_R}{q_\perp^2 (q_\perp^2 + m_D^2)} \int \frac{d^3 p}{(2\pi)^3} \frac{p - p_z}{p} [2C_A n_B(p)(1 + n_B(p')) + 4N_f T_f n_F(p)(1 - n_F(p'))], \quad (18)$$

with $p' = p + \frac{q_\perp^2 + 2q_\perp \cdot p}{2(p-p_z)}$ and displays the following asymptotic behaviors

$$C_{\text{QCD}}^{\text{LO}}(q_\perp) = g^2 T C_R \begin{cases} \frac{m_D^2 - g^2 T^2 C_A \frac{q_\perp}{16T}}{q_\perp^2 (q_\perp^2 + m_D^2)}, & q_\perp \ll gT, \\ \frac{g^2 T^2}{q_\perp^4} \frac{\zeta(3)}{\zeta(2)} \left(1 + \frac{N_f}{4}\right), & q_\perp \gg gT. \end{cases} \quad (19)$$

Next-to-leading order (NLO) corrections are of order g^5 and arise from infrared corrections that are suppressed by an additional factor of $m_D \sim g$, which can be calculated in EQCD [31]. Similar to the treatment of the non-perturbative kernel, the NLO broadening kernel is computed using perturbative results for the soft contributions from EQCD and supplying the hard contribution by a matching [31]. Specifically,

$$C_{\text{QCD}}^{\text{NLO}}(q_\perp) = C_{\text{EQCD}}^{\text{LO}}(q_\perp) + C_{\text{EQCD}}^{\text{NLO}}(q_\perp) + C_{\text{QCD}}^{\text{pert}}(q_\perp) - C_{\text{subtr}}^{\text{pert}}(q_\perp), \quad (20)$$

where the leading and next-to-leading order contributions from soft modes are given by [31, 40, 43]

$$C_{\text{EQCD}}^{\text{LO}}(q_\perp) = C_R g^2 T \frac{m_D^2}{q_\perp^2 (q_\perp^2 + m_D^2)}, \quad (21)$$

$$\begin{aligned} \frac{C_{\text{EQCD}}^{\text{NLO}}(q_\perp)}{g^4 T^2 C_R C_A} &= \frac{7}{32 q_\perp^3} + \frac{-m_D - 2 \frac{q_\perp^2 - m_D^2}{q_\perp} \tan^{-1}\left(\frac{q_\perp}{m_D}\right)}{4\pi (q_\perp^2 + m_D^2)^2} \\ &+ \frac{m_D - \frac{q_\perp^2 + 4m_D^2}{2q_\perp} \tan^{-1}\left(\frac{q_\perp}{2m_D}\right)}{8\pi q_\perp^4} \\ &- \frac{\tan^{-1}\left(\frac{q_\perp}{m_D}\right)}{2\pi q_\perp (q_\perp^2 + m_D^2)} + \frac{\tan^{-1}\left(\frac{q_\perp}{2m_D}\right)}{2\pi q_\perp^3} \\ &+ \frac{m_D}{4\pi (q_\perp^2 + m_D^2)} \left[\frac{3}{q_\perp^2 + 4m_D^2} - \frac{2}{(q_\perp^2 + m_D^2)} - \frac{1}{q_\perp^2} \right], \quad (22) \end{aligned}$$

and if not stated otherwise, we employ the leading order perturbative expressions for m_D (see Eq. (27)) when evaluating the LO and NLO kernels.

D. Numerical results

We display the different momentum broadening kernels $C_{\text{QCD}}(b_\perp)$ in Fig. 1 where the perturbative kernels are computed using the same coupling g as the one for $T = 500\text{MeV}$ in Tab I. The top panel presents the kernel $C_{\text{QCD}}(b_\perp)$ in impact parameter space, where bands represent the uncertainty in spline definition as discussed in [1]. We use the same color coding when presenting the momentum broadening kernel $C_{\text{QCD}}(q_\perp)$ in momentum space in the bottom panel of Fig. 1, where the bands represent the transformation of the different splines in the band from the left panel. We also show the limiting behaviors in the infrared in Eq. (16) and ultra-violet in

Eq. (17), as well as the LO and NLO kernels in Eqns. (18) and (20). Strikingly, when expressing T/C_R as a function of q_\perp/gT both data sets at $T = 250, 500\text{MeV}$ display very similar behavior. As expected, in the IR the rate follows a $(1/q_\perp^3)$ behavior similar to the NLO kernel; however they differ by a prefactor due to the difference in the string tension. For intermediate values of $q_\perp/(gT)$, the momentum broadening kernel determined from EQCD lattice data falls below the LO and NLO results. In the UV limit, all kernels display the same $(1/q_\perp^4)$ behavior, associated with the contribution from hard scatterings in Eq. (4).

III. MEDIUM-INDUCED SPLITTING RATES

Equipped with the broadening kernel $C(q_\perp)$ in momentum space, we now proceed to compute the rate of medium-induced radiation. Starting point of the rate calculation is the formal expression [9, 10, 12]

$$\frac{dP_{bc}^a}{dz} = \frac{g^2 P_{bc}^a(z)}{4\pi P^2 z^2 (1-z)^2} \text{Re} \int_0^\infty dt_1 \int_{t_1}^\infty dt \int_{\mathbf{p}, \mathbf{q}} \mathbf{q} \cdot \mathbf{p} [G(t, \mathbf{q}; t_1, \mathbf{p}) - (\text{vac})], \quad (23)$$

which describe the total probability of (nearly) collinear in-medium splitting of the particle a with momentum P into particles b and c with momentum zP and $(1-z)P$ respectively. The propagator $G(t, \mathbf{q}; t_1, \mathbf{p})$ satisfies the evolution equation

$$(\partial_t + i\delta E(\mathbf{q}) + \Gamma_3(t))G(t, \mathbf{q}; t_1, \mathbf{p}) = 0, \quad (24)$$

with initial condition

$$G(t_1, \mathbf{q}; t_1, \mathbf{p}) = \frac{1}{4P^2 z^2 (1-z)^2} (2\pi)^2 \delta^{(2)}(\mathbf{p} - \mathbf{q}). \quad (25)$$

The energy is given by

$$\delta E(\mathbf{p}) \equiv \frac{\mathbf{p}^2}{2Pz(1-z)} + \frac{m_z^2}{2zP} + \frac{m_{1-z}^2}{2(1-z)P} - \frac{m_1^2}{2P}, \quad (26)$$

where m_i are the medium induced mass of the particles carrying momentum fraction i . Throughout this analysis we will use the leading order perturbative expressions

$$m_{\infty, g}^2 = \frac{m_D^2}{2} = g^2 T^2 \left(\frac{N_c}{6} + \frac{N_f}{12} \right), \quad (27)$$

$$m_{\infty, q}^2 = g^2 T^2 \frac{(N_c^2 - 1)}{8N_c^2}, \quad (28)$$

with $N_c = 3$ and $N_f = 3$. The collisional broadening of the propagator can be expressed as the following collision

integral

$$\begin{aligned} \Gamma_3(t) \circ G(t, \mathbf{p};) = & \\ \frac{1}{C_R} \int_{\mathbf{q}} C_{\text{QCD}}(t, \mathbf{q}) & \left\{ C_1 [G(t, \mathbf{p};) - G(t, \mathbf{p} - \mathbf{q};)] \right. \\ & + C_z [G(t, \mathbf{p};) - G(t, \mathbf{p} + z\mathbf{q};)] \\ & \left. + C_{1-z} [G(t, \mathbf{p};) - G(t, \mathbf{p} + (1-z)\mathbf{q};)] \right\}, \end{aligned} \quad (29)$$

where the color factors are defined as

$$C_1 = \frac{C_z^R + C_{1-z}^R - C_1^R}{2}, \quad C_z = \frac{C_1^R + C_{1-z}^R - C_z^R}{2}, \quad (30)$$

$$C_{1-z} = \frac{C_1^R + C_z^R - C_{1-z}^R}{2}, \quad (31)$$

and C_z^R is the Casimir of the particle with momentum fraction z , i.e. $C_R = C_A = N_c$ for gluons and $C_R = C_F = \frac{(N_c^2 - 1)}{2N_c}$ for quarks. By following [12], one can use an integration by part to rewrite the following integral

$$\begin{aligned} & \int_{t_1}^{\infty} dt G(t, \mathbf{q}; t_1, \mathbf{p}) \\ &= \int_{t_1}^{\infty} dt \left[\frac{d}{dt} \left(\frac{e^{-i\delta E(\mathbf{q})t}}{-i\delta E(\mathbf{q})} \right) \right] e^{+i\delta E(\mathbf{q})t} G(t, \mathbf{q}; t_1, \mathbf{p}), \end{aligned} \quad (32)$$

such that upon use of the evolution equation for the propagator in Eq. (24), the expression simplifies to

$$\begin{aligned} & \int_{t_1}^{\infty} dt G(t, \mathbf{q}; t_1, \mathbf{p}) \\ &= \frac{1}{-i\delta E(\mathbf{q})} [G(\infty, \mathbf{q}; t_1, \mathbf{p}) - G(t_1, \mathbf{q}; t_1, \mathbf{p})] \\ &+ \int_{t_1}^{\infty} dt \frac{i}{\delta E(\mathbf{q})} \Gamma_3(t) \circ G(t, \mathbf{q}; t_1, \mathbf{p}). \end{aligned} \quad (33)$$

Now, as argued by [12], the terms in the second line of Eq. (33) do not contribute to the rate, as the first vanishes in the limit $t \rightarrow \infty$ due to rapid oscillations, while the second term merely correspond the initial condition in Eq. (25) and thus cancels against the vacuum subtraction in Eq. (23). By inserting Eq. (33) into Eq. (23) re-arranging the order of integrations, and performing a time derivative w.r.t. t , the rate of medium-induced radiation can be compactly expressed in the form [12]

$$\begin{aligned} \frac{d\Gamma_{bc}^a}{dz}(P, z, t) &= \frac{g^2 P_{bc}^a(z)}{4\pi P^2 z^2 (1-z)^2} \\ \text{Re} \int_0^t dt_1 \int_{\mathbf{p}, \mathbf{q}} & \frac{i\mathbf{q} \cdot \mathbf{p}}{\delta E(\mathbf{q})} \Gamma_3(t) \circ G(t, \mathbf{q}; t_1, \mathbf{p}). \end{aligned} \quad (34)$$

1. Expressing the rate using wave function

By introducing the wave function

$$\vec{\psi}(\mathbf{p}, t, t_1) = \int_{\mathbf{q}} \frac{i\mathbf{q}}{\delta E(\mathbf{q})} \Gamma_3(t) \circ G(t, \mathbf{q}; t_1, \mathbf{p}), \quad (35)$$

we may further compactify the expression for the rate as follows

$$\begin{aligned} \frac{d\Gamma_{bc}^a}{dz}(P, z, t) &= \frac{g^2 P_{bc}^a(z)}{4\pi P^2 z^2 (1-z)^2} \text{Re} \int_0^t dt_1 \int_{\mathbf{p}} \mathbf{p} \cdot \vec{\psi}(\mathbf{p}, t, t_1). \end{aligned} \quad (36)$$

Exploiting the linearity of the evolution equation (24), one finds that the evolution equation for the wave function w.r.t. t_1 is given by

$$[\partial_{t_1} - i\delta E(\mathbf{p}) - \Gamma_3(t_1) \circ] \vec{\psi}(\mathbf{p}, t, t_1) = 0, \quad (37)$$

which needs to be solved backward in time t_1 for $t > t_1 > 0$, with the initial condition

$$\vec{\psi}(\mathbf{p}, t, t_1) = \int_{\mathbf{q}} \frac{i\mathbf{q}}{\delta E(\mathbf{q})} \Gamma_3 \circ (2\pi)^2 \delta^2(\mathbf{p} - \mathbf{q}), \quad (38)$$

$$= \Gamma_3(t) \circ \frac{i\mathbf{p}}{\delta E(\mathbf{p})}, \quad (39)$$

While the above re-arrangements can always be performed, we will in the following consider the radiative emission rates in a static QCD plasma, where $\Gamma_3(t) = \Gamma_3$ and $\vec{\psi}(\mathbf{p}, t, t_1) = \vec{\psi}(\mathbf{p}, \Delta t)$ only depends on separation $\Delta t = t - t_1$.

We proceed to factor out the physical scales by defining the dimensionless variables

$$\Delta \tilde{t} = \frac{m_D^2}{2Pz(1-z)} \Delta t, \quad \tilde{q} = \frac{q}{m_D}, \quad \tilde{p} = \frac{p}{m_D}, \quad (40)$$

where $m_D^2/2Pz(1-z)$ is the inverse formation time of a splitting with small momentum transfer $\sim m_D$, and the energy becomes

$$\begin{aligned} \delta \tilde{E}(\tilde{\mathbf{p}}) &= \frac{2Pz(1-z)}{m_D^2} \delta E(\mathbf{p}), \\ &= \frac{\tilde{\mathbf{p}}^2}{2Pz(1-z)} + (1-z) \frac{m_z^2}{m_D^2} + z \frac{m_{1-z}^2}{m_D^2} - z(1-z) \frac{m_1^2}{m_D^2}. \end{aligned} \quad (41)$$

By factoring out the parametric dependencies of the broadening kernel as $\tilde{C}(\tilde{\mathbf{q}}) = \frac{m_D^2}{C_R g^2 T} C(\mathbf{q})$, one finds

$$\Gamma_3 = g^2 T \tilde{\Gamma}_3. \quad (43)$$

Now, expressing the wave function as

$$\vec{\psi}(\mathbf{p}, \Delta t) = g^2 T \frac{2Pz(1-z)}{m_D} \vec{\psi}(\tilde{\mathbf{p}}, \Delta \tilde{t}). \quad (44)$$

the initial conditions can then be compactly expressed in terms of the dimensionless variables as

$$\vec{\psi}(\tilde{\mathbf{p}}, \Delta\tilde{t} = 0) = \tilde{\Gamma}_3(t) \circ \frac{i\tilde{\mathbf{p}}}{\delta\tilde{E}(\tilde{\mathbf{p}})} . \quad (45)$$

The evolution equation for the dimensionless wave function takes the form

$$\left[\partial_{\Delta\tilde{t}} + \delta\tilde{E}(\tilde{\mathbf{p}}) + \lambda \tilde{\Gamma}_3(t) \circ \right] \vec{\psi}(\tilde{\mathbf{p}}, \Delta\tilde{t}) = 0 , \quad (46)$$

where $\lambda = g^2 T \frac{2Pz(1-z)}{m_D^2}$ counts the number of small angle scatterings per formation time of a splitting with small momentum transfer $\sim m_D$, and the splitting rate becomes

$$\frac{d\Gamma_{bc}^a}{dz}(P, z, \tilde{t}) = \frac{g^4 T P_{bc}^a(z)}{\pi} \text{Re} \int_0^{\tilde{t}} d\Delta\tilde{t} \int_{\tilde{\mathbf{p}}} \tilde{\mathbf{p}} \cdot \vec{\psi}(\tilde{\mathbf{p}}, \Delta\tilde{t}) . \quad (47)$$

Still following earlier works [12], the numerical determination of the rate can be further simplified by exploiting the isotropy of the wave-function in isotropic plasmas and introducing the transformation to the interaction picture. Defining

$$\tilde{\psi}_I(\tilde{\mathbf{p}}, \Delta\tilde{t}) = e^{i\delta\tilde{E}(\tilde{\mathbf{p}})\Delta\tilde{t}} \tilde{\mathbf{p}} \cdot \vec{\psi}(|\tilde{\mathbf{p}}|, \Delta\tilde{t}) , \quad (48)$$

$$\vec{\psi}(|\tilde{\mathbf{p}}|, \Delta\tilde{t}) = e^{-i\delta\tilde{E}(\tilde{\mathbf{p}})\Delta\tilde{t}} \frac{\tilde{\mathbf{p}}}{\tilde{p}^2} \tilde{\psi}_I(\tilde{\mathbf{p}}, \Delta\tilde{t}) , \quad (49)$$

one finds that $\tilde{\psi}_I(\tilde{\mathbf{p}}, \Delta\tilde{t})$ follows the evolution equation

$$\left[\partial_{\Delta\tilde{t}} + \lambda e^{i\delta\tilde{E}(\tilde{\mathbf{p}})\Delta\tilde{t}} \tilde{\mathbf{p}} \cdot \tilde{\Gamma}_3 \circ e^{-i\delta\tilde{E}(\tilde{\mathbf{p}})\Delta\tilde{t}} \frac{\tilde{\mathbf{p}}}{\tilde{p}^2} \right] \tilde{\psi}_I(\tilde{\mathbf{p}}, \Delta\tilde{t}) = 0 , \quad (50)$$

with the initial condition

$$\tilde{\psi}_I(\tilde{\mathbf{p}}, \Delta\tilde{t} = 0) = \tilde{\mathbf{p}} \cdot \tilde{\Gamma}_3 \circ \frac{i\tilde{\mathbf{p}}}{\delta\tilde{E}(\tilde{\mathbf{p}})} , \quad (51)$$

and the splitting rate can be compactly expressed as

$$\frac{d\Gamma_{bc}^a}{dz} = \frac{g^4 T P_{bc}^a(z)}{\pi} \text{Re} \int_0^{\tilde{t}} d\Delta\tilde{t} \int_{\tilde{\mathbf{p}}} e^{-i\delta\tilde{E}(\tilde{\mathbf{p}})\Delta\tilde{t}} \tilde{\psi}_I(\tilde{\mathbf{p}}, \Delta\tilde{t}) , \quad (52)$$

which is the form of the equation that we use for our numerical determination of the medium induced splitting rate for fixed values of P and z .

We use a logarithmic grid to discretize the momentum \tilde{p} and employ a standard numerical integration from the GNU scientific library [44] to obtain the initial wave function $\tilde{\psi}_I(\tilde{\mathbf{p}}, \Delta\tilde{t} = 0)$ from Eq. (51) at each point. Subsequently, the discretized wave functions $\tilde{\psi}_I(\tilde{\mathbf{p}}, \Delta\tilde{t})$ are evolved using an Euler scheme, where we use a spline interpolation to interpolate the discrete wave function when numerically integrating the collision integral in

Eq. (50). Eventually, the two-dimensionally tabulated values of the wave function $\tilde{\psi}_I(\tilde{\mathbf{p}}, \Delta\tilde{t})$ are made continuous using a two-dimensional spline and integrated numerically with the CUBA library [45] to obtain the rate in Eq. (52). We note that for the next-to-leading perturbative, as well as for the non-perturbative momentum broadening kernel, the $1/q_\perp^3$ IR behavior can lead to instabilities when evolving the coupled set of evolution equations. However, this problem can be resolved by separating the soft and hard contributions to momentum broadening, and treating the soft contributions in an expansion of the momentum transfer q_\perp to perform the integrations analytically, as discussed in detail in Appendix B.

Even though the numerical solution for the rate can be obtained at all scales for a highly energetic parton, one can get away with using approximations in certain regimes which simplifies the calculation drastically. Numerous approximations have been developed in the literature [9] [5] [22–24] [13], during the following sections we will review the latest developments together with some traditional approximations, which we will compare to the full rate in Figure. 4.

A. Opacity expansion

Simplification to the rate occur, when the medium is short and the hard particle does not frequently interact with the medium. In this regime, the rate can be computed perturbatively in an expansion in the number of interactions N with the medium. This expansion is also known as the Gyulassy, Levai and Vitev (GLV) approximation¹ [16, 46]. It is easier to compute the expansion in the interaction picture introduced earlier, the wave function for the first order ($N = 1$) is directly the initial condition defined in Eq. (51) as we already take one scattering in the definition of the wave function

$$\tilde{\psi}_I^{(1)}(\tilde{\mathbf{p}}) = \tilde{\mathbf{p}} \cdot \tilde{\Gamma}_3 \circ \frac{i\tilde{\mathbf{p}}}{\delta\tilde{E}(\tilde{\mathbf{p}})} . \quad (53)$$

By inserting the wave function into the definition of the rate in Eq. (52), one obtains

$$\begin{aligned} \frac{d\Gamma_{bc}^a}{dz} \Big|_{N=1} (P, z, \tilde{t}) &= \frac{g^4 T P_{bc}^a(z)}{\pi} \text{Re} \int_0^{\tilde{t}} d\Delta\tilde{t} \int_{\tilde{\mathbf{p}}} e^{-i\delta\tilde{E}(\tilde{\mathbf{p}})\Delta\tilde{t}} \tilde{\mathbf{p}} \cdot \tilde{\Gamma}_3 \circ \frac{i\tilde{\mathbf{p}}}{\delta\tilde{E}(\tilde{\mathbf{p}})} . \\ & \quad (54) \end{aligned}$$

¹ We note here that in contrast to the traditional GLV approximation we will not neglect thermal masses, and we will not take the soft gluon approximation.

The time integration can be done analytically and one finds [16, 46]

$$\left. \frac{d\Gamma_{bc}^a}{dz} \right|_{N=1} (P, z, \tilde{t}) = \frac{g^4 T P_{bc}^a(z)}{\pi} \int_{\tilde{\mathbf{p}}} \frac{1 - \cos(\delta \tilde{E}(\tilde{\mathbf{p}}) \tilde{t})}{\delta \tilde{E}(\tilde{\mathbf{p}})} \tilde{\mathbf{p}} \cdot \tilde{\Gamma}_3 \circ \frac{i\tilde{\mathbf{p}}}{\delta \tilde{E}(\tilde{\mathbf{p}})}. \quad (55)$$

B. Resummed opacity expansion

Besides the straight opacity expansion, the authors of [25] developed a resummation that tries to capture additional re-scatterings with the medium. During this section we will present this procedure, starting with the second order ($N = 2$) correction to the wave function which obeys the following evolution equation

$$\partial_{\Delta \tilde{t}} \tilde{\psi}_I^{(2)}(\tilde{\mathbf{p}}, s) = -\lambda e^{i\delta \tilde{E}(\tilde{\mathbf{p}})s} \tilde{\mathbf{p}} \cdot \tilde{\Gamma}_3 \circ e^{-i\delta \tilde{E}(\tilde{\mathbf{p}})s} \frac{\tilde{\mathbf{p}}}{\tilde{p}^2} \tilde{\psi}_I^{(1)}(\tilde{\mathbf{p}}), \quad (56)$$

with initial condition $\tilde{\psi}_I^{(2)}(\tilde{\mathbf{p}}, \Delta \tilde{t} = 0) = 0$. Integrating with respect to time, one finds

$$\tilde{\psi}_I^{(2)}(\tilde{\mathbf{p}}, \Delta \tilde{t}) = -\lambda \int_0^{\Delta \tilde{t}} ds e^{i\delta \tilde{E}(\tilde{\mathbf{p}})s} \tilde{\mathbf{p}} \cdot \tilde{\Gamma}_3 \circ e^{-i\delta \tilde{E}(\tilde{\mathbf{p}})s} \frac{\tilde{\mathbf{p}}}{\tilde{p}^2} \tilde{\psi}_I^{(1)}(\tilde{\mathbf{p}}). \quad (57)$$

Explicitly, the correction is given by

$$\begin{aligned} \tilde{\psi}_I^{(2)}(\tilde{\mathbf{p}}, \Delta \tilde{t}) = & -\lambda \int_0^{\Delta \tilde{t}} ds e^{i\delta \tilde{E}(\tilde{\mathbf{p}})s} \tilde{\mathbf{p}} \cdot \int_{\tilde{\mathbf{q}}} \left[C_1 \tilde{C}(\tilde{\mathbf{q}}) + \frac{C_z}{z^2} \tilde{C}\left(\frac{\tilde{\mathbf{q}}}{z}\right) + \frac{C_{1-z}}{(1-z)^2} \tilde{C}\left(\frac{\tilde{\mathbf{q}}}{1-z}\right) \right] \\ & \left[e^{-i\delta \tilde{E}(\tilde{\mathbf{p}})s} \frac{\tilde{\mathbf{p}}}{\tilde{p}^2} \tilde{\psi}_I^{(1)}(\tilde{\mathbf{p}}) - e^{-i\delta \tilde{E}(\tilde{\mathbf{p}}-\tilde{\mathbf{q}})s} \frac{\tilde{\mathbf{p}}-\tilde{\mathbf{q}}}{|\tilde{\mathbf{p}}-\tilde{\mathbf{q}}|^2} \tilde{\psi}_I^{(1)}(\tilde{\mathbf{p}}-\tilde{\mathbf{q}}) \right], \end{aligned} \quad (58)$$

where we have utilized a change of variable in the $\tilde{\mathbf{q}}$ integral to combine the different terms in the collision integral in Eq. (29). Now following [25] and considering the difference

$$\tilde{\psi}_I^{(1)}(\tilde{\mathbf{p}}) - e^{i(\delta \tilde{E}(\tilde{\mathbf{p}}) - \delta \tilde{E}(\tilde{\mathbf{p}}-\tilde{\mathbf{q}}))s} \frac{\tilde{\mathbf{p}}^2 - \tilde{\mathbf{p}} \cdot \tilde{\mathbf{q}}}{|\tilde{\mathbf{p}} - \tilde{\mathbf{q}}|^2} \tilde{\psi}_I^{(1)}(\tilde{\mathbf{p}} - \tilde{\mathbf{q}}), \quad (59)$$

one concludes, that for small momentum transfer ($\tilde{q} \ll 1$), the two terms cancel each other, while for larger momentum transfer ($\tilde{q} \gg 1$) the phase factor oscillates rapidly and the second term does not contribute significantly to the integral. By introducing a cut-off scale μ^2 and dropping the second term in Eq. (59), one can then approximately keep track of the contributions $\tilde{\Sigma}(\mu^2) = \int_{\tilde{q}^2 > \mu^2} \tilde{C}(\tilde{\mathbf{q}})$ with large momentum transfer, yielding

$$\tilde{\psi}_I^{(2)}(\tilde{\mathbf{p}}, \Delta \tilde{t}) = -\lambda \int_0^{\Delta \tilde{t}} ds \tilde{\psi}_I^{(1)}(\tilde{\mathbf{p}}) \tilde{\Sigma}_3(\mu^2, z), \quad (60)$$

where $\tilde{\Sigma}_3(\mu^2, z) = \left[C_1 \tilde{\Sigma}(\mu^2) + C_z \tilde{\Sigma}(\mu^2/z^2) + C_{1-z} \tilde{\Sigma}(\mu^2/(1-z)^2) \right]$. Inserting Eqns. (51) and (57) into (52), the expansion of the splitting rate is now given by

$$\begin{aligned} \left. \frac{d\Gamma_{bc}^a}{dz} \right|_{N=X} (P, z, \tilde{t}) &= \frac{g^4 T P_{bc}^a(z)}{\pi} \text{Re} \int_0^{\tilde{t}} d\Delta \tilde{t} \int_{\tilde{\mathbf{p}}} e^{-i\delta \tilde{E}(\tilde{\mathbf{p}}) \Delta \tilde{t}} \tilde{\psi}_I^{(1)}(\tilde{\mathbf{p}}) \\ &+ \frac{g^4 T P_{bc}^a(z)}{\pi} \text{Re} \int_0^{\tilde{t}} d\Delta \tilde{t} \int_0^{\Delta \tilde{t}} ds \\ &\times \int_{\tilde{\mathbf{p}}} e^{-i\delta \tilde{E}(\tilde{\mathbf{p}}) \Delta \tilde{t}} \tilde{\psi}_I^{(1)}(\tilde{\mathbf{p}}) \left(-\lambda \tilde{\Sigma}_3(\mu^2, z) \right) + \dots \end{aligned} \quad (61)$$

After performing the time integral (ds), one finds

$$\begin{aligned} \left. \frac{d\Gamma_{bc}^a}{dz} \right|_{N=X} (P, z, \tilde{t}) &= \frac{g^4 T P_{bc}^a(z)}{\pi} \text{Re} \int_0^{\tilde{t}} d\Delta \tilde{t} \int_{\tilde{\mathbf{p}}} e^{-i\delta \tilde{E}(\tilde{\mathbf{p}}) \Delta \tilde{t}} \tilde{\psi}_I^{(1)}(\tilde{\mathbf{p}}) \\ &+ \frac{g^4 T P_{bc}^a(z)}{\pi} \text{Re} \int_0^{\tilde{t}} d\Delta \tilde{t} \\ &\times \int_{\tilde{\mathbf{p}}} e^{-i\delta \tilde{E}(\tilde{\mathbf{p}}) \Delta \tilde{t}} \tilde{\psi}_I^{(1)}(\tilde{\mathbf{p}}) \left(-\lambda \tilde{\Sigma}_3(\mu^2, z) \Delta \tilde{t} \right) + \dots \end{aligned} \quad (62)$$

One notices that subsequent terms with additional time integration will exponentiate, yielding the final result

$$\begin{aligned} \left. \frac{d\Gamma_{bc}^a}{dz} \right|_{N=X} (P, z, \tilde{t}) &= \frac{g^4 T P_{bc}^a(z)}{\pi} \text{Re} \int_0^{\tilde{t}} d\Delta \tilde{t} \int_{\tilde{\mathbf{p}}} e^{-(i\delta \tilde{E}(\tilde{\mathbf{p}}) + \lambda \tilde{\Sigma}_3(\mu^2, z)) \Delta \tilde{t}} \tilde{\psi}_I^{(1)}(\tilde{\mathbf{p}}), \end{aligned} \quad (63)$$

where following [25], we employed $\mu^2 = \tilde{p}^2$ for the cutoff scale.

C. Harmonic Oscillator expansion

When the typical energy evolved in the radiation is much larger than the medium temperature ($Pz(1-z) \ll T$), the formation time is large so that multiple soft scatterings have to be resummed. By treating the multiple soft scatterings in diffusion approximation, the evolution equation for the Green's function can be re-cast into the form of a harmonic oscillator type equation which can be solved analytically [47]. Rather than using this approximation only, we will make use of recent calculations which go beyond this simple harmonic oscillator limit by treating the hard scatterings as a perturbative correction on top of the resummed infinitely many soft scatterings [22–24]. Here, we will only compute the first correction,

i.e. a single hard scattering in addition to many soft scatterings.

Starting with the short-distance behavior defined in Eq. (7), one can introduce a scale Q^2 to evaluate the logarithm and separate it as follows

$$\bar{C}(b_\perp) = \frac{1}{C_R} C(b_\perp) \quad (64)$$

$$= \frac{g^4 T^3}{16\pi} \mathcal{N} b_\perp^2 \ln \left(\frac{4Q^2}{\xi m_D^2} \right) + \frac{g^4 T^3}{16\pi} \mathcal{N} b_\perp^2 \ln \left(\frac{1}{Q^2 b_\perp^2} \right) \quad (65)$$

where $\xi = 4 \frac{g^4 T^2}{m_D^2} e^{-4\pi \frac{q_0}{C_R g^4 T^3 \mathcal{N}}} \simeq 0.1702$ for $T = 500 \text{ MeV}$.

Based on this separation, the Harmonic oscillator (HO) kernel is now defined as the first part of Eq. (65), i.e.

$$\bar{C}^{HO}(b_\perp) = \frac{g^4 T^3}{16\pi} \mathcal{N} b_\perp^2 \ln \left(\frac{4Q^2}{\xi m_D^2} \right), \quad (66)$$

which is used to calculate the Green's function subject to multiple soft-scatterings, while the remainder is treated perturbatively. Instead of using only the short-distance limit, i.e. $\bar{C}^{\text{pert}}(b_\perp) = \frac{g^4 T^3}{16\pi} \mathcal{N} b_\perp^2 \ln \left(\frac{1}{Q^2 b_\perp^2} \right)$, it is better to define the correction to the kernel as the difference

$$\bar{C}^{\text{pert}}(b_\perp) = \bar{C}(b_\perp) - \bar{C}^{HO}(b_\perp), \quad (67)$$

where we use the full definition of $\bar{C}(b_\perp)$, i.e. the numerical spline. The radiation spectrum will also be separate to the sum of the HO and the first correction

$$\frac{dI^{NLO}}{dz}(P, z, t) = \frac{dI^{HO}}{dz}(P, z, t) + \frac{dI^{(1)}}{dz}(P, z, t), \quad (68)$$

where the correction is computed using a first order opacity expansion with the kernel $C^{\text{pert}}(b_\perp)$ around the harmonic oscillator solution. Following [22–24], the scale Q^2 is the typical momentum of the radiated quanta defined self-consistently by using

$$Q^2(P, z) = \sqrt{Pz(1-z)\hat{q}_{\text{eff}}(Q^2)}, \quad (69)$$

$$\hat{q}_{\text{eff}}(Q^2) = \frac{g^4 T^3}{4\pi} \mathcal{N} [C_1 + C_z z^2 + C_{1-z}(1-z)^2] \times \ln \left(\frac{4Q^2}{\xi m_D^2} \right), \quad (70)$$

where $\hat{q}_{\text{eff}}(Q^2)$ is the coefficient of the three-body interaction term Γ_3 , obtained by plugging $C^{HO}(b_\perp)$ in Eq. (29).

1. Leading Order

Using $C^{HO}(b_\perp)$ the rate equations can be solved analytically [5, 8, 10], historically the result was obtained in terms of the spectrum

$$\frac{dI^{HO}}{dz}(P, z, t) = \frac{g^2 P_{bc}^a(z)}{4\pi^2} \ln |\cos \Omega t|, \quad (71)$$

where we define the frequency

$$\Omega = \frac{1-i}{2} \sqrt{\frac{\hat{q}_{\text{eff}}(Q^2)}{Pz(1-z)}}. \quad (72)$$

By applying a time derivative [12], one obtains the leading order harmonic oscillator rate

$$\frac{dI^{HO}}{dz}(P, z, t) = -\frac{g^2 P_{bc}^a(z)}{4\pi^2} \text{Re } \Omega \tan \Omega t. \quad (73)$$

2. Next to Leading order

While the leading order HO term can be seen as a resummation of multiple soft scatterings with the medium, the next-to-leading order correction introduces the effect of one ‘hard’ scattering with the medium. One obtains the correction by making use of the separation in Eq. (68), which translates to a separation of the propagators

$$G(t, \mathbf{b}_\perp; t_1, \mathbf{p}) = G^{HO}(t, \mathbf{b}_\perp; t_1, \mathbf{y}) + G^{(1)}(t, \mathbf{b}_\perp; t_1, \mathbf{y}). \quad (74)$$

By inserting the full propagator into the evolution Eq. (24), and using the fact that the propagator $G^{HO}(t, \mathbf{q}; t_1, \mathbf{p})$ is solution to the equation

$$\left[i\partial_t + \frac{\partial_{\mathbf{b}_\perp^2}}{2Pz(1-z)} + M_{\text{eff}} + i\Gamma_3^{HO}(\mathbf{b}_\perp) \right] G^{HO}(\mathbf{b}_\perp, t; \mathbf{y}, t_1) = i\delta(t-t_1)\delta^{(2)}(\mathbf{b}_\perp - \mathbf{y}). \quad (75)$$

One finds the evolution equation of the next-to-leading order propagator $G^{(1)}(t, \mathbf{b}_\perp; t_1, \mathbf{y})$

$$\left[i\partial_t + \frac{\partial_{\mathbf{b}_\perp^2}}{2Pz(1-z)} + M_{\text{eff}} + i\Gamma_3^{HO}(\mathbf{b}_\perp) \right] G^{(1)}(\mathbf{b}_\perp, t; \mathbf{y}, t_1) = -i\Gamma_3^{\text{pert}}(\mathbf{b}_\perp) G^{HO}(\mathbf{b}_\perp, t; \mathbf{y}, t_1), \quad (76)$$

where one neglects next-to-next-to-leading order terms $\propto \Gamma_3^{\text{pert}}(\mathbf{b}_\perp) G^{(1)}(\mathbf{b}_\perp, t; \mathbf{y}, t_1)$. Strikingly, the evolution equation can be solved analytically to obtain the spectrum [22–24]

$$\begin{aligned} & \frac{dI^{(1)}}{dz}(P, z, t) \\ &= \frac{g^2 P_{bc}^a(z)}{4\pi^2} \text{Re} \int_0^t ds \int_0^\infty \frac{2du}{u} [C_1 \bar{C}^{\text{pert}}(u) + C_z \bar{C}^{\text{pert}}(zu) \\ & \quad + C_{1-z} \bar{C}^{\text{pert}}((1-z)u)] e^{k^2(s)u^2}, \end{aligned} \quad (77)$$

$$\begin{aligned} &= \frac{g^2 P_{bc}^a(z)}{4\pi^2} \text{Re} \int_0^t ds \int \frac{2du}{u} \bar{C}^{\text{pert}}(u) \left[C_1 e^{k^2(s)u^2} + C_z e^{\frac{k^2(s)}{z^2}u^2} \right. \\ & \quad \left. + C_{1-z} e^{\frac{k^2(s)}{(1-z)^2}u^2} \right], \end{aligned} \quad (78)$$

where we define

$$k^2(s) = \frac{iPz(1-z)\Omega}{2} [\cot \Omega s - \tan \Omega(t-s)]. \quad (79)$$

When presenting numerical results for the NLO harmonic oscillator approximation, we compute the integrated spectrum in Eq. (68) and subsequently perform a numerical derivative w.r.t. t to obtain the rate shown in Fig. 4.

IV. NUMERICAL RESULTS

We now turn to the discussion of numerical results for the in-medium radiation rate. We numerically obtain the rate for the different (LO,NLO,NP) broadening kernels $C(q_\perp)$ as described in detail in App. B; the software to calculate the rates is publicly available at [49]. We illustrate our results at the example of the radiation of a gluon by a parent quark of energy $P = 300T$ in an equilibrium medium with constant temperature $T = 500\text{MeV}$. We present our results for the rate $d\Gamma/dz$ in Figure 2 as a function of time t for three different momentum fractions $z = 0.05, 0.25, 0.5$ and in Figure 3 as a function of momentum fraction z for four different times $t = 0.15, 0.4, 1, 4\text{fm}/c$. Different curves in each panel of Figs. 2 and 3 show the rates obtained using the non-perturbatively (NP) determined $C(q_\perp)$, along with the results for the leading order (LO) and next-to-leading order (NLO) perturbative collision kernel (c.f. Sec. II). Insets at the bottom of each graphic displays the ratio to the LO results.

With regards to time dependence in Fig. 2, one finds that the splitting rates exhibit a linear behavior at early times ($t \lesssim \frac{2Pz(1-z)}{m_D^2}$) and quickly saturate at later times where the splitting rate is given by the infinite medium rate. We indicate the infinite medium rate by a gray dashed line, which can be determined entirely in impact parameter space (c.f. [1]), and thus provides an important validation of the numerical procedure. When comparing the results obtained for the different collision kernels, we observe that the non-perturbative result starts lower than the LO rates before it settles above the LO and below the NLO.

When considering the z dependence of the rate in Fig. 3 one observes that finite size effects lead to a significant suppression of the rate of quasi-democratic ($z \sim 1/2$) splittings compared to the infinite medium rates ($t = \infty$). While at early times, the non-perturbatively determined rate $d\Gamma/dz$ is suppressed compared to the LO rate for all momentum fractions z , it starts to rise above the LO results as the rates for soft ($z \ll 1$) and hard ($z \sim 1$) branchings approach the infinite medium limit.

Notably, we find that in both Figs. 2 and 3 the result for the non-perturbative kernel does not depart from a band of $\pm 50\%$ around LO, while the NLO result can become over $2\times$ larger than the LO result.

We also computed the various approximations to the splitting rates discussed in Sec. III. In Figures 4 and 5 we compare the full in-medium rates to the first order opacity expansion ($N = 1$), the resummed opac-

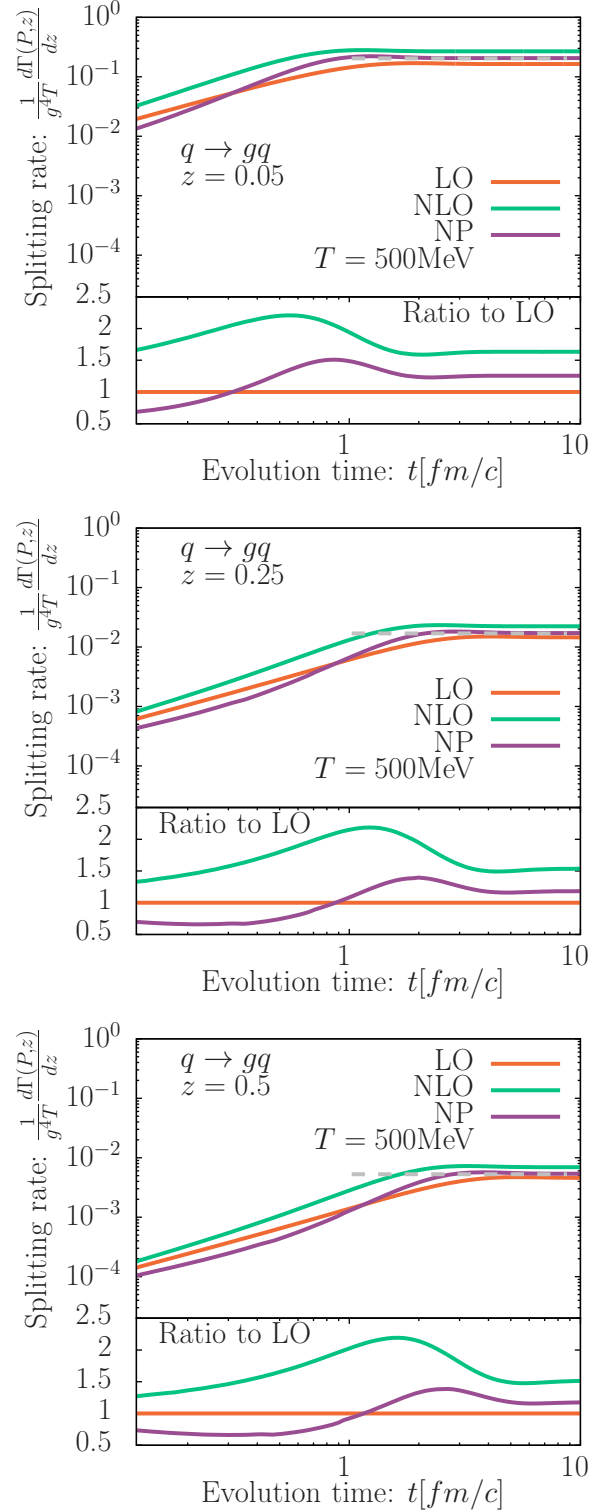


FIG. 2. Splitting rate for the medium-induced emission of a gluon from a parent quark with energy $P = 300T$ in an equilibrium plasma with temperature $T = 250, 500\text{MeV}$ as a function of the evolution time t . Each panel represent a different gluon momentum fraction $z = 0.05, 0.25, 0.5$ from top to bottom. We compare calculation done using the different collisional broadening kernel as shown in Fig. 1 (the temperature and coupling constant for the perturbative results are matched to the $T = 500\text{MeV}$ data in Tab. I). The lower panel of each plot displays the ratio to the LO results.

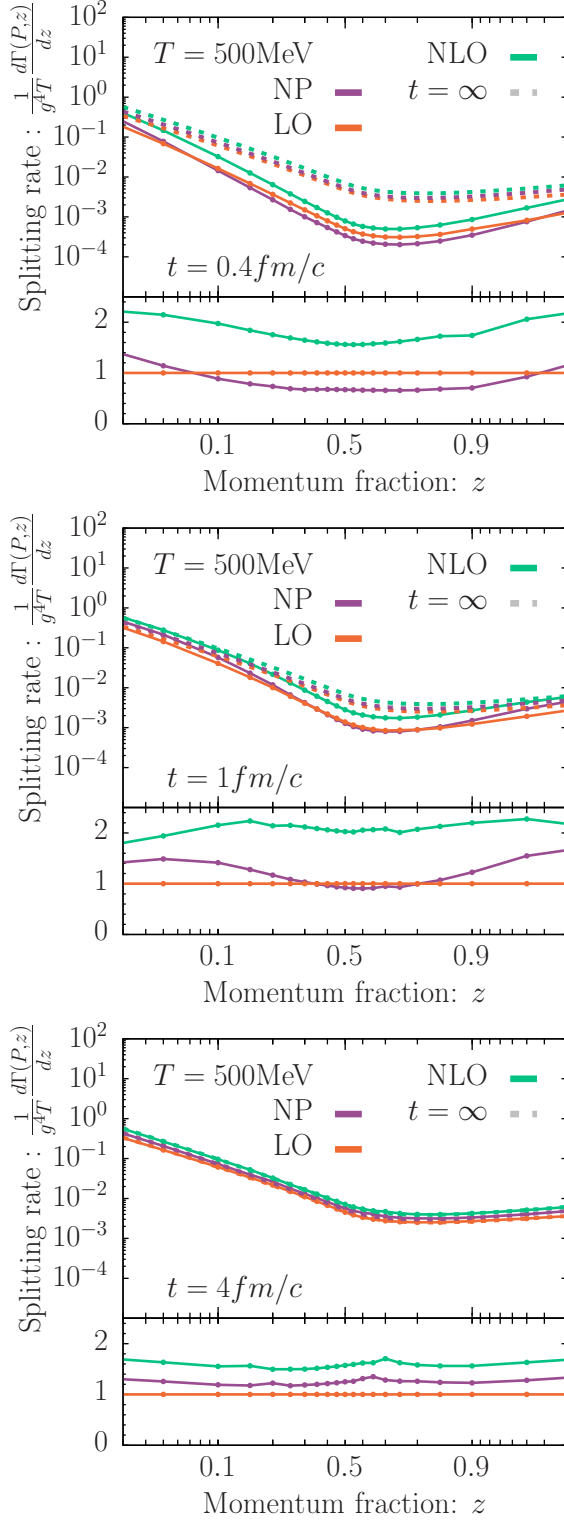


FIG. 3. Splitting rate for the medium-induced emission of a gluon from a parent quark with energy $P = 300T$ in an equilibrium medium with temperature $T = 500\text{MeV}$ as a function of momentum fraction of the radiated gluon z . Different panels show the rate $d\Gamma/dz$ at fixed times $t = 0.4, 1, 4\text{fm}/c$ from top to bottom. The lower panel of each plot shows the ratio to the splitting rate for the LO momentum broadening kernel. Dashed lines correspond to the (AMY) splitting rates [48] in an infinite medium [1]

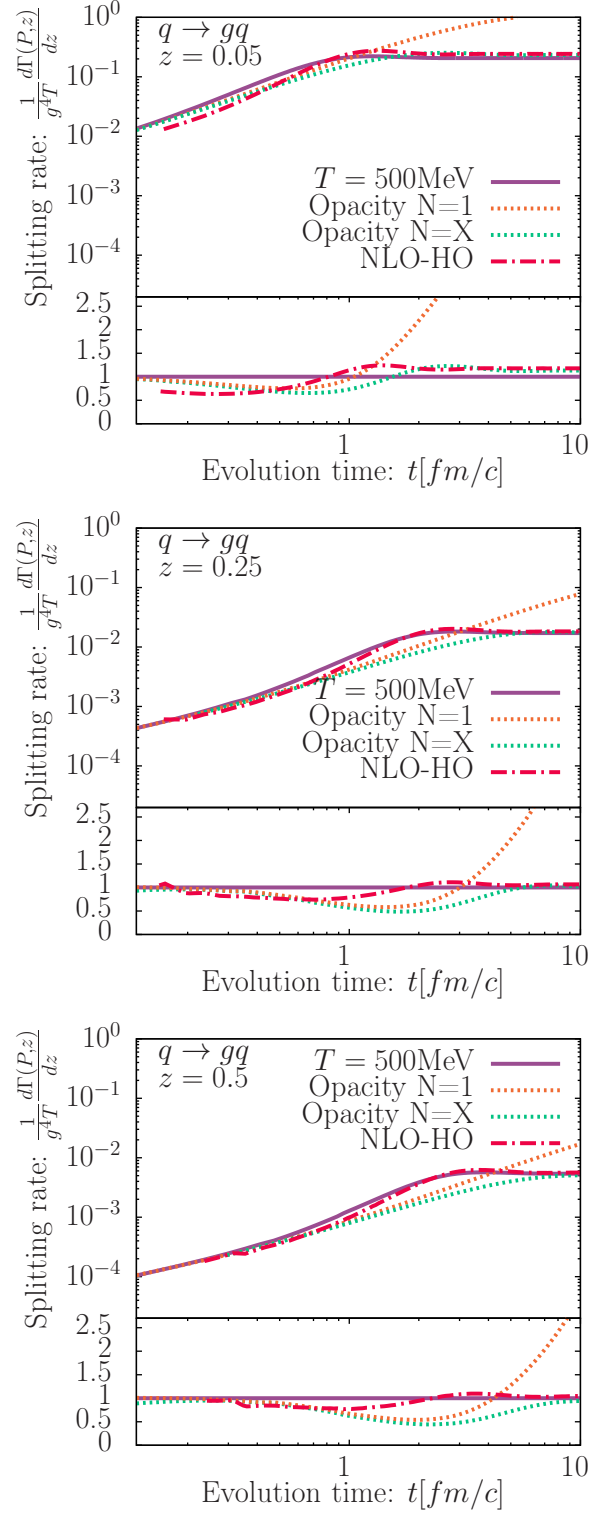


FIG. 4. Splitting rate for the medium-induced emission of a gluon from a parent quark with energy $P = 300T$ as a function of the evolution time t . Each panel represent a different gluon momentum fraction $z = 0.05, 0.25, 0.5$ from top to bottom. We compare different approximations of the in-medium splitting rate, namely the opacity expansion at $N = 1$ Eq.(55), the resummed opacity rate of Eq. (63) ($N = X$) and the NLO expansion around the Harmonic Oscillator Eq. (68) (NLO-HO) to the full result ($T = 500\text{MeV}$). Note that all results are obtained with the non-perturbative collision kernel. The lower panel of each plot displays the ratio to the full rate.

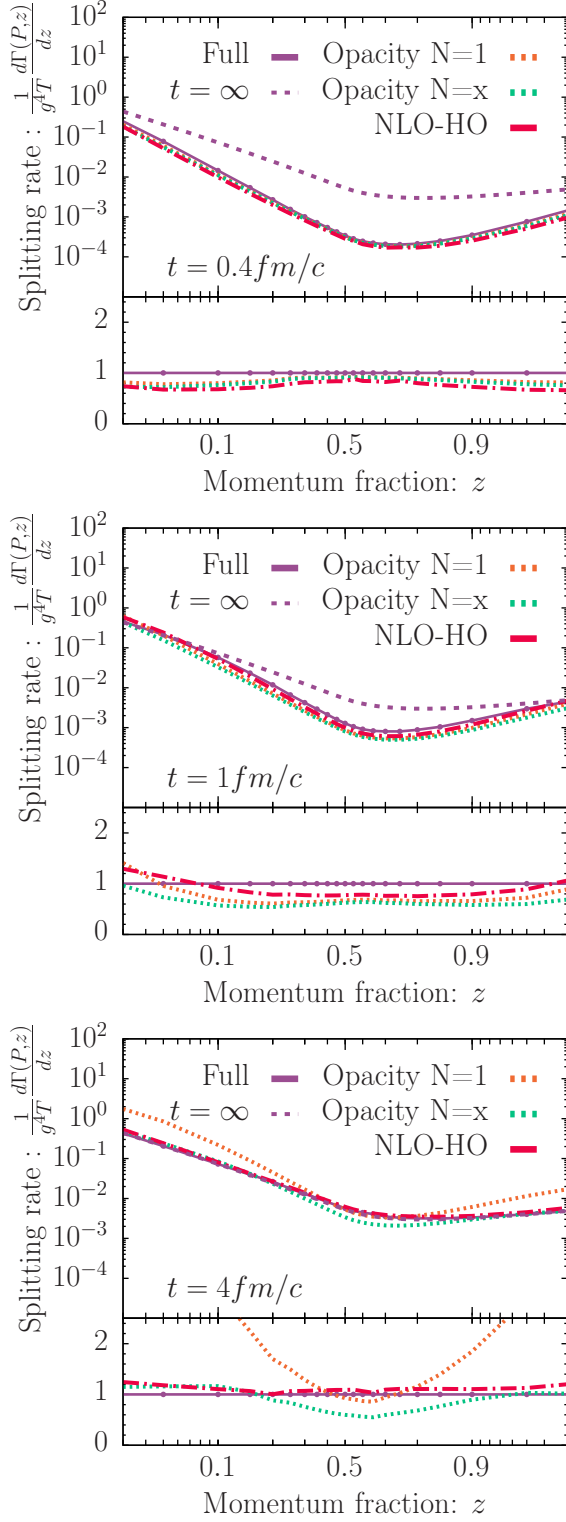


FIG. 5. Splitting rate for the medium-induced emission of a gluon from a parent quark with energy $P = 300T$ as a function of momentum fraction of the radiated gluon z . Different panels show the rate $d\Gamma/dz$ at fixed times $t = 0.4, 1, 4 fm/c$. We compare different approximations of the in-medium splitting rate, namely the opacity expansion at $N = 1$ Eq.(55), the resummed opacity rate of Eq. (63) ($N = X$) and the NLO expansion around the Harmonic Oscillator Eq. (68) (NLO-HO) to the full result ($T = 500 MeV$). Note that all results are obtained with the non-perturbative collision kernel. The lower panel of each plot shows the ratio to the full splitting rate.

ity expansion ($N = X$), and the next-to-leading order expansion around the HO (NLO-HO) approximation. We emphasize that in all cases we employ the same non-perturbative broadening kernel $C_{QCD}(q_\perp)$ at $T = 500 MeV$, such that any differences are solely due to underlying approximations in the calculation of the rate. Different panels in Fig. 4 show the results for $d\Gamma/dz$ as a function of time for three gluon momentum fractions $z = 0.05, 0.25, 0.5$; the bottom insets in each panel represent the ratio of the respective approximation to the full in-medium splitting rate. We observe that, as expected, the early time linear behavior is captured by the opacity expansion since the parton does not have sufficient time to re-interact with the medium. However, soon after the leading order ($N = 1$) opacity expansion starts to overestimate the rate, while the resummed ($N = X$) opacity expansion is able to reproduce the rate rather well even at late times especially for soft splittings ($z \ll 0.5$). Similarly, the NLO expansion around the HO also performs fairly well at all times, especially if one considers quasi-democratic splittings ($z \sim 1/2$).

With regards to the z dependence shown in 5, we find that, as pointed out above, the $N = X$ opacity dependence works particularly well at small/large momentum fractions z , while the NLO expansion around the HO is typically most accurate for quasi-democratic splittings ($z \sim 1/2$). Nevertheless, the overall z dependence is well reproduced by both approaches, and the deviations from the full rate behave fairly uniformly as a function of z as can be inferred from the ratios in the insets. Evidently, the leading order opacity expansion is only applicable for times much smaller than the formation time, and fails particularly badly for highly asymmetric splittings on large time scales.

By comparing the effect of various approximations in Figs. 4 and 5, with the impact of the different LO, NLO and NP collision kernels in Figs. 2 and 3, we find that the choice of the broadening kernel is clearly more impactful for the calculation of the in-medium splitting rates.

V. CONCLUSION

Building on the determination of the collisional broadening kernel $C_{QCD}(\mathbf{b}_\perp)$ in [1], we performed a Fourier transform of $C_{QCD}(\mathbf{b}_\perp)$, to determine the non-perturbative broadening kernel $C_{QCD}(\mathbf{q}_\perp)$ in momentum space in order to compute radiative emissions rates in a QCD medium of finite extent.

We presented results for the in-medium splitting rates obtained with the non-perturbative collision kernel and compared them to the results obtained with leading and next-to-leading order perturbative collision kernels, as well as with different approximations of the in-medium splitting rates, which are commonly employed in the literature. While approximations to the splitting rate calculation are quite effective in reproducing the rate within their respective range of validity, differences between the

LO kernel, which is usually used in phenomenological studies of jet quenching, and the non-perturbative kernel can easily be on the order of 30%. We conclude that, while for sophisticated numerical simulations one can reconstruct the full rate to obtain precise results, for (semi-)analytical calculations a combination of the resummed opacity and NLO-HO rates is likely sufficient, as theoretical improvements mostly rely on the precise knowledge of the collisional broadening kernel.

With regards to the phenomenological applications of our work, we note that the collisional broadening kernel and in-medium splitting rates obtained in this paper can be incorporated into a study of jet quenching either using a kinetic approach [50–52] or with a MonteCarlo simulations [53–56]. Similarly, one could also utilize the same broadening kernel to include non-perturbative contributions to the elastic scatterings. We finally note that a recent study using the same EQCD setting obtained non-perturbative contributions to the thermal masses [38] and it would be interesting to investigate their impact on the rate calculation specifically and jet quenching in general.

ACKNOWLEDGEMENT

We thank Guy D. Moore and Niels Schlusser for insightful discussions, collaboration on our previous work [1] and their help in performing the Fourier transform of the momentum broadening kernel. This work is supported in part by the Deutsche Forschungsgemeinschaft (DFG, German Research Foundation) through the CRC-TR 211 ‘Strong-interaction matter under extreme conditions’– project number 315477589 – TRR 211 and the German Bundesministerium für Bildung und Forschung (BMBF) through Grant No. 05P21PBAA. The authors also gratefully acknowledge computing time provided by the Paderborn Center for Parallel Computing (PC2).

Appendix A: Hankel transformation

Below we provide details of the procedure followed to obtain the Hankel transform of the momentum broadening kernel.

1. Numerical implementation of the Hankel transformation

To perform the numerical integration in Eq. (13), we split the integral using the zeros $\{x_i\}$ of the Bessel func-

tion ($J_1(x_i) = 0$) as follows

$$\Delta C^{\text{NP}}(q_\perp) = \frac{2\pi}{q_\perp} \sum_{i=0}^{\infty} \int_{x_i/q_\perp}^{x_{i+1}/q_\perp} db_\perp b_\perp J_1(b_\perp q_\perp) \times \frac{d}{db_\perp} \Delta C^{\text{NP}}(b_\perp). \quad (\text{A1})$$

Let us define the series

$$A_n = \int_{x_i/q_\perp}^{x_{i+1}/q_\perp} db_\perp b_\perp J_1(b_\perp q_\perp) \frac{d}{db_\perp} \Delta C^{\text{NP}}(b_\perp). \quad (\text{A2})$$

The Hankel transform is then given by the sum $A = \sum_{n=0}^{\infty} A_n$, however, this sum is slowly convergent. The convergence can be accelerated using a method known as Shanks transformation [57], where one defines the series

$$A = \lim_{n \rightarrow \infty} S(A_n), \quad (\text{A3})$$

$$= \lim_{n \rightarrow \infty} A_{n+1} - \frac{(A_{n+1} - A_n)^2}{(A_{n+1} - A_n) - (A_n - A_{n-1})}. \quad (\text{A4})$$

The result is then obtained by truncating the sum when we obtain convergence up to a small tolerance threshold, i.e. when $\left| \frac{S(A_{n+1})}{S(A_n)} - 1 \right| \leq 10^{-8}$.

2. Transformation of the short-distance behavior

At short-distances the broadening kernel follows a similar behavior to the LO kernel, which is the short-distance limit of

$$C(b_\perp) = \frac{C_R g^4 T^3 \mathcal{N}}{8\pi m_D^2} [\gamma_e + \log(m_D b_\perp / 2) + K_0(m_D b_\perp)]. \quad (\text{A5})$$

In momentum space this broadening kernel is given by [58]

$$C(q_\perp) = \frac{C_R g^4 T^3 \mathcal{N}}{m_D^2} \frac{m_D^2}{q_\perp^2 (q_\perp^2 + m_D^2)}. \quad (\text{A6})$$

Since we are only interested in the leading UV behavior, provided by the $b^2 \log(b)$ term, the non-perturbative broadening kernel will follow the same behavior as the LO kernel

$$C^{\text{UV}}(q_\perp) = \frac{C_R g^4 T^3 \mathcal{N}}{8\pi} \frac{8\pi}{q_\perp^4}. \quad (\text{A7})$$

3. Transformation of the long-distance behavior

We proceed to transform the long-distance behavior given in Eq. (6). Let us first consider the Hankel transformation of the linear function

$$C(b_\perp) = A + B b_\perp. \quad (\text{A8})$$

The constant term leads to a delta function $\delta^{(2)}(q_\perp)$ in momentum space which can be discarded, and the linear term will lead to

$$C(q_\perp) = B \frac{2\pi}{q_\perp^3}. \quad (\text{A9})$$

Note that in order to verify this identity, it is actually easier to compute the following inverse transform

$$\begin{aligned} & \int \frac{d^2 q_\perp}{(2\pi)^2} \frac{2\pi}{q_\perp^3} (1 - e^{iq_\perp \cdot \mathbf{b}_\perp}) \\ &= \frac{1}{2\pi} \int_{-\infty}^{\infty} dx \int_{-\infty}^{\infty} dy \frac{1}{(x^2 + y^2)^{3/2}} (1 - e^{ixb_\perp}), \\ &= \frac{1}{2\pi} \int_{-\infty}^{\infty} dx \frac{2}{x^2} (1 - \cos xb_\perp) = b_\perp. \end{aligned} \quad (\text{A10})$$

Appendix B: Numerical implementation

Below we provide some additional details on the numerical calculation of the splitting rate for finite media following the approach of [12]. We employ a forward Euler scheme, to evolve the wave function from $\Delta\tilde{t} = 0$ to $\Delta\tilde{t} = \tilde{t}$ according to the differential equation (50) and use our results to perform the integral in Eq. (52).

1. Separating the soft scale

When solving the evolution equation using the NLO and non-perturbative broadening kernels, we find that the $1/q^3$ behavior at small momentum leads to numerical instabilities. In order to stabilize this evolution, we will consider the soft interactions in the collision integral separately. Starting with Eq. (29), we rewrite the collision integral using the interaction picture and combine the different momentum integrals using variable change to find

$$\begin{aligned} & \tilde{\Gamma}_3 \circ \tilde{\psi}(\tilde{p}) \\ &= e^{i\delta\tilde{E}(\tilde{p})\Delta\tilde{t}} \tilde{\mathbf{p}} \cdot \\ & \int_{\tilde{\mathbf{q}}} \left[C_1 \tilde{C}(\tilde{\mathbf{q}}) + \frac{C_z}{z^2} \tilde{C}\left(\frac{\tilde{\mathbf{q}}}{z}\right) + \frac{C_{1-z}}{(1-z)^2} \tilde{C}\left(\frac{\tilde{\mathbf{q}}}{1-z}\right) \right] \\ & \left[e^{-i\delta\tilde{E}(\tilde{p})\Delta\tilde{t}} \frac{\tilde{\mathbf{p}}}{\tilde{p}^2} \tilde{\psi}_I(\tilde{p}) - e^{-i\delta\tilde{E}(|\tilde{\mathbf{p}}-\tilde{\mathbf{q}}|\Delta\tilde{t})} \frac{\tilde{\mathbf{p}}-\tilde{\mathbf{q}}}{|\tilde{\mathbf{p}}-\tilde{\mathbf{q}}|^2} \tilde{\psi}_I(|\tilde{\mathbf{p}}-\tilde{\mathbf{q}}|) \right], \end{aligned} \quad (\text{B1})$$

By introducing an intermediate cut-off μ in the momentum exchange \tilde{q} , the collision integral is separated to hard and soft interactions

$$C[\tilde{\psi}_I] = C_{\text{hard}}[\tilde{\psi}_I] + C_{\text{soft}}[\tilde{\psi}_I]. \quad (\text{B2})$$

The soft interaction can be treated in a diffusion approximation using an expansion in momentum exchange \tilde{q} .

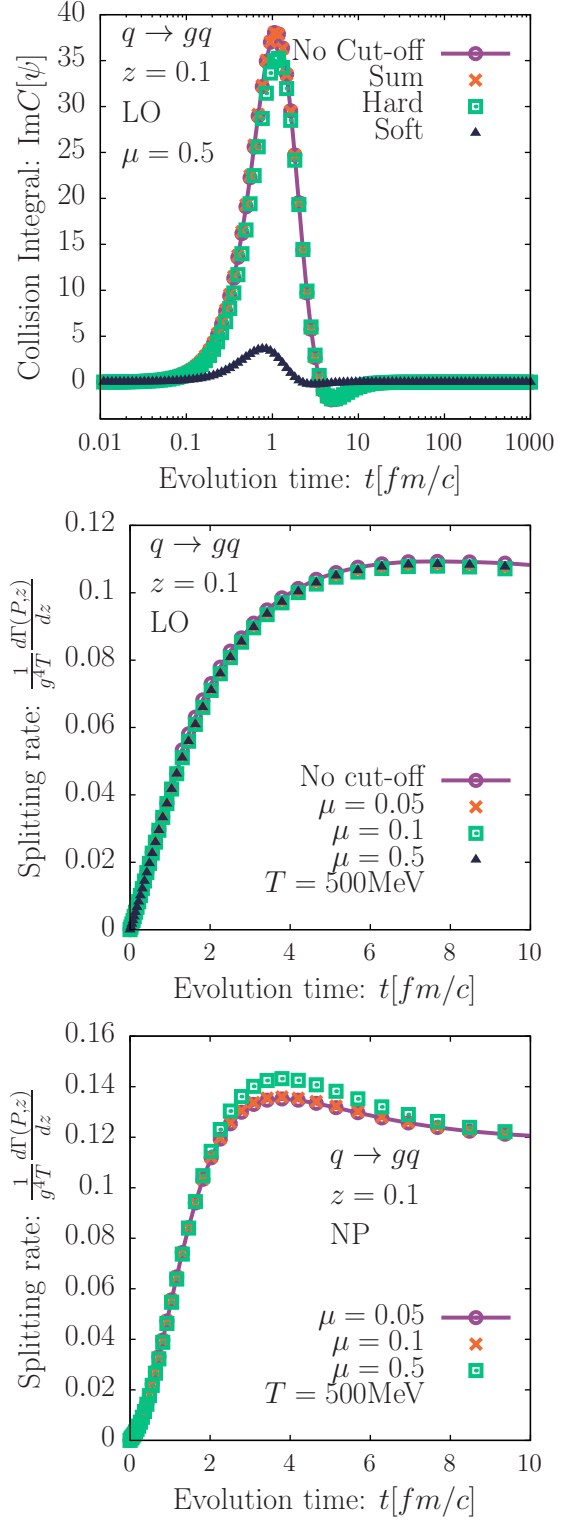


FIG. 6. Validation of the separation into soft and hard components, by varying the cut-off $\mu = 0.05, 0.1, 0.5$ in the calculation for a quark with momentum $P = 300T$ radiating a gluon with momentum fraction $z = 0.1$. (top) Comparison of the imaginary part of the initial integral using the LO broadening kernel, where we show the separation of the hard and diffusion part of the collision integral for $\mu = 0.5$ and compare the sum to the full collision integral without separating the soft-scales. The in-medium splitting rate using the perturbative LO (middle) or the non-perturbative (bottom) broadening kernel do not show any significant dependence on the choice of the cut-off scale.

We specifically expand the following term from Eq. (50) of the collision integral

$$\begin{aligned} \frac{\tilde{p}^2 - \tilde{\mathbf{p}} \cdot \tilde{\mathbf{q}}}{|\tilde{\mathbf{p}} - \tilde{\mathbf{q}}|^2} \tilde{\psi}_I(|\tilde{\mathbf{p}} - \tilde{\mathbf{q}}|) &= \tilde{\psi}_I(\tilde{p}) + \frac{\tilde{q}}{\tilde{p}} \cos \theta \left[\tilde{\psi}_I(\tilde{p}) - \tilde{p} \tilde{\psi}'_I(\tilde{p}) \right] \\ &+ \frac{q^2}{2\tilde{p}^2} \left[2 \cos 2\theta \tilde{\psi}_I(\tilde{p}) \right. \\ &\left. + \tilde{p}(1 - 3 \cos^2 \theta) \tilde{\psi}'_I(\tilde{p}) + \tilde{p}^2 \cos^2 \theta \tilde{\psi}''_I(\tilde{p}) \right], \end{aligned} \quad (\text{B3})$$

where θ is the angle between $\tilde{\mathbf{p}}$ and $\tilde{\mathbf{q}}$. Plugging the expansion to the collision integral and performing the angular integral, we find

$$\begin{aligned} C_{\text{soft}}[\tilde{\psi}_I] &= \tilde{\psi}_I(\tilde{p}) \left(I_1^{(0)}(\tilde{p}, \Delta\tilde{t}) - I_2(\tilde{p}, \Delta\tilde{t}) - I_1^{(3)}(\tilde{p}, \Delta\tilde{t}) \right) \\ &+ \frac{p}{2} \tilde{\psi}'_I(\tilde{p}) \left(2I_2(\tilde{p}, \Delta\tilde{t}) - I_2^{(3)}(\tilde{p}, \Delta\tilde{t}) \right) - \frac{p^2}{2} \tilde{\psi}''_I(\tilde{p}) I_3(\tilde{p}, \Delta\tilde{t}), \end{aligned} \quad (\text{B4})$$

where I_i are the following integral moments

$$\begin{aligned} I_1^{(0)}(\tilde{p}, \Delta\tilde{t}) &= \frac{1}{2\pi} \int_0^\mu d\tilde{q} \mathcal{C}(\tilde{q}, z) \left[1 - e^{-i\Delta\tilde{t}\tilde{q}^2} \right. \\ &\quad \left. \times \mathcal{J}_0(2\Delta\tilde{t}\tilde{p}\tilde{q}) \right], \end{aligned} \quad (\text{B5})$$

$$\begin{aligned} I_1^{(3)}(\tilde{p}, \Delta\tilde{t}) &= \frac{-1}{2\pi} \int_0^\mu d\tilde{q} \mathcal{C}(\tilde{q}, z) \frac{\tilde{q}^2}{\tilde{p}^2} e^{-i\Delta\tilde{t}\tilde{q}^2} \\ &\quad \times \mathcal{J}_2(2\Delta\tilde{t}\tilde{p}\tilde{q}), \end{aligned} \quad (\text{B6})$$

$$\begin{aligned} I_2(\tilde{p}, \Delta\tilde{t}) &= \frac{1}{2\pi} \int_0^\mu d\tilde{q} \mathcal{C}(\tilde{q}, z) \frac{\tilde{q}}{\tilde{p}} i e^{-i\Delta\tilde{t}\tilde{q}^2} \\ &\quad \times \mathcal{J}_1(2\Delta\tilde{t}\tilde{p}\tilde{q}), \end{aligned} \quad (\text{B7})$$

$$\begin{aligned} I_2^{(3)}(\tilde{p}, \Delta\tilde{t}) &= \frac{1}{2\pi} \int_0^\mu d\tilde{q} \mathcal{C}(\tilde{q}, z) \frac{\tilde{q}^2}{\tilde{p}^2} e^{-i\Delta\tilde{t}\tilde{q}^2} \left[\frac{3}{2\Delta\tilde{t}\tilde{p}\tilde{q}} \right. \\ &\quad \left. \times \mathcal{J}_1(2\Delta\tilde{t}\tilde{p}\tilde{q}) - 2\mathcal{J}_0(2\Delta\tilde{t}\tilde{p}\tilde{q}) \right], \end{aligned} \quad (\text{B8})$$

$$\begin{aligned} I_3(\tilde{p}, \Delta\tilde{t}) &= \frac{1}{2\pi} \int_0^\mu d\tilde{q} \mathcal{C}(\tilde{q}, z) \frac{\tilde{q}^2}{\tilde{p}^2} e^{-i\Delta\tilde{t}\tilde{q}^2} \left[\frac{1}{2\Delta\tilde{t}\tilde{p}\tilde{q}} \right. \\ &\quad \left. \times \mathcal{J}_1(2\Delta\tilde{t}\tilde{p}\tilde{q}) - \mathcal{J}_2(2\Delta\tilde{t}\tilde{p}\tilde{q}) \right], \end{aligned} \quad (\text{B9})$$

where $\mathcal{J}_i(x)$ are the Bessel functions of the first kind and

$$\mathcal{C}(\tilde{q}, z) = \tilde{q} \left[C_1 \tilde{C}(\tilde{q}) + \frac{C_z}{z^2} \tilde{C}\left(\frac{\tilde{q}}{z}\right) + \frac{C_{1-z}}{(1-z)^2} \tilde{C}\left(\frac{\tilde{q}}{1-z}\right) \right] \quad (\text{B10})$$

We perform the integrals in Eqns. (B5-B9) numerically and tabulate them for a fixed time step $\Delta\tilde{t}$. Combining the soft component with the hard component, then makes up the full collision integral in Eq. 50, which can be used to evolve the wave function. While the hard component is easily evolved using an Euler explicit scheme, we employ an implicit scheme for the soft component to deal with instabilities. We show in Fig. 6 the effect of the choice of the cut-off scale $\mu \sim 0.05 - 0.5$ on the evaluation of the collision integral (top) as well as for the in-medium splitting computed using both the LO (middle) and non-perturbative broadening kernel (bottom). The top panel displays how, for a relatively large cut-off $\mu = 0.5$ the soft and hard part sum to recover the full collision integral, i.e. the result obtained without separating the soft scales for the LO perturbative broadening kernel. We observe in the middle and bottom panels how for sufficiently small cut-off scales $\mu \ll 1$ the change of the cut-off scale has almost no effect on the resulting in-medium splittings rates. We note for completeness that the results shown in Sec. IV are obtained for a value $\mu = 0.05$.

-
- [1] G. D. Moore, S. Schlichting, N. Schlusser, and I. Soudi, (2021), arXiv:2105.01679 [hep-ph].
- [2] J. Bjorken, (1982).
- [3] M. Gyulassy and X.-n. Wang, Nucl. Phys. B **420**, 583 (1994), arXiv:nucl-th/9306003.
- [4] R. Baier, Y. L. Dokshitzer, S. Peigne, and D. Schiff, Phys. Lett. B **345**, 277 (1995), arXiv:hep-ph/9411409.
- [5] B. G. Zakharov, JETP Lett. **63**, 952 (1996), arXiv:hep-ph/9607440.
- [6] L. D. Landau and I. Pomeranchuk, Dokl. Akad. Nauk Ser. Fiz. **92**, 535 (1953).
- [7] A. B. Migdal, Phys. Rev. **103**, 1811 (1956).
- [8] R. Baier, Y. L. Dokshitzer, A. H. Mueller, S. Peigne, and D. Schiff, Nucl. Phys. B **483**, 291 (1997), arXiv:hep-ph/9607355.
- [9] R. Baier, Y. L. Dokshitzer, A. H. Mueller, S. Peigne, and D. Schiff, Nucl. Phys. B **484**, 265 (1997), arXiv:hep-ph/9608322.
- [10] B. G. Zakharov, JETP Lett. **65**, 615 (1997), arXiv:hep-ph/9704255.
- [11] P. B. Arnold, G. D. Moore, and L. G. Yaffe, JHEP **06**, 030 (2002), arXiv:hep-ph/0204343.
- [12] S. Caron-Huot and C. Gale, Phys. Rev. C **82**, 064902 (2010), arXiv:1006.2379 [hep-ph].
- [13] C. Andres, L. Apolinário, and F. Dominguez, (2020), 10.1007/JHEP07(2020)114, arXiv:2002.01517 [hep-ph].
- [14] B. G. Zakharov, Phys. Atom. Nucl. **61**, 838 (1998), [Yad. Fiz.61,924(1998)], arXiv:hep-ph/9807540 [hep-ph].
- [15] U. A. Wiedemann and M. Gyulassy, Nucl. Phys. B **560**, 345 (1999), arXiv:hep-ph/9906257.
- [16] M. Gyulassy, P. Levai, and I. Vitev, Nucl. Phys. B **571**, 197 (2000), arXiv:hep-ph/9907461.
- [17] C. A. Salgado and U. A. Wiedemann, Phys. Rev. D **68**, 014008 (2003), arXiv:hep-ph/0302184.
- [18] J.-P. Blaizot, F. Dominguez, E. Iancu, and Y. Mehtar-Tani, JHEP **01**, 143 (2013), arXiv:1209.4585 [hep-ph].
- [19] L. Apolinário, N. Armesto, J. G. Milhano, and C. A. Salgado, JHEP **02**, 119 (2015), arXiv:1407.0599 [hep-ph].
- [20] M. D. Sievert, I. Vitev, and B. Yoon, Phys. Lett. B **795**, 502 (2019), arXiv:1903.06170 [hep-ph].
- [21] M. Gyulassy, P. Levai, and I. Vitev, Phys. Rev. Lett. **85**, 5535 (2000), arXiv:nucl-th/0005032.

- [22] Y. Mehtar-Tani, JHEP **07**, 057 (2019), arXiv:1903.00506 [hep-ph].
- [23] Y. Mehtar-Tani and K. Tywoniuk, JHEP **06**, 187 (2020), arXiv:1910.02032 [hep-ph].
- [24] J. Barata and Y. Mehtar-Tani, (2020), arXiv:2004.02323 [hep-ph].
- [25] C. Andres, F. Dominguez, and M. Gonzalez Martinez, JHEP **03**, 102 (2021), arXiv:2011.06522 [hep-ph].
- [26] Y. Mehtar-Tani, J. G. Milhano, and K. Tywoniuk, Int. J. Mod. Phys. A **28**, 1340013 (2013), arXiv:1302.2579 [hep-ph].
- [27] S. Cao and X.-N. Wang, (2020), arXiv:2002.04028 [hep-ph].
- [28] A. D. Linde, Phys. Lett. **96B**, 289 (1980).
- [29] E. Braaten and A. Nieto, Phys. Rev. **D51**, 6990 (1995), arXiv:hep-ph/9501375 [hep-ph].
- [30] J. Casalderrey-Solana and D. Teaney, JHEP **04**, 039 (2007), arXiv:hep-th/0701123 [hep-th].
- [31] S. Caron-Huot, Phys. Rev. D **79**, 065039 (2009), arXiv:0811.1603 [hep-ph].
- [32] M. Panero, K. Rummukainen, and A. Schäfer, Phys. Rev. Lett. **112**, 162001 (2014), arXiv:1307.5850 [hep-ph].
- [33] M. D’Onofrio, A. Kurkela, and G. D. Moore, JHEP **03**, 125 (2014), arXiv:1401.7951 [hep-lat].
- [34] G. D. Moore and N. Schlusser, Phys. Rev. **D100**, 034510 (2019), arXiv:1905.09708 [hep-lat].
- [35] G. D. Moore and N. Schlusser, Phys. Rev. **D101**, 014505 (2020), arXiv:1911.13127 [hep-lat].
- [36] P. B. Arnold, G. D. Moore, and L. G. Yaffe, JHEP **01**, 030 (2003), arXiv:hep-ph/0209353 [hep-ph].
- [37] U. A. Wiedemann, Nucl. Phys. B **588**, 303 (2000), arXiv:hep-ph/0005129.
- [38] G. D. Moore and N. Schlusser, Phys. Rev. D **102**, 094512 (2020), arXiv:2009.06614 [hep-lat].
- [39] J. Ghiglieri and H. Kim, JHEP **12**, 049 (2018), arXiv:1809.01349 [hep-ph].
- [40] P. B. Arnold and W. Xiao, Phys. Rev. D **78**, 125008 (2008), arXiv:0810.1026 [hep-ph].
- [41] M. Laine, Eur. Phys. J. C **72**, 2233 (2012), arXiv:1208.5707 [hep-ph].
- [42] M. Laine and Y. Schroder, JHEP **03**, 067 (2005), arXiv:hep-ph/0503061 [hep-ph].
- [43] P. Aurenche, F. Gelis, G. D. Moore, and H. Zaraket, JHEP **12**, 006 (2002), arXiv:hep-ph/0211036 [hep-ph].
- [44] M. Galassi, J. Davies, J. Theiler, B. Gough, G. Jungman, M. Booth, and F. Rossi, “Gnu scientific library - reference manual,”.
- [45] T. Hahn, Comput. Phys. Commun. **168**, 78 (2005), arXiv:hep-ph/0404043.
- [46] M. Gyulassy, P. Levai, and I. Vitev, Nucl. Phys. B **594**, 371 (2001), arXiv:nucl-th/0006010.
- [47] P. B. Arnold, Phys. Rev. **D79**, 065025 (2009), arXiv:0808.2767 [hep-ph].
- [48] P. B. Arnold, G. D. Moore, and L. G. Yaffe, JHEP **05**, 051 (2003), arXiv:hep-ph/0302165.
- [49] S. Schlichting and I. Soudi, [*GitHub/Finite-Medium-Splitting-Rates-Using-Non-perturbative-Kernel*], (2021).
- [50] Y. Mehtar-Tani and S. Schlichting, JHEP **09**, 144 (2018), arXiv:1807.06181 [hep-ph].
- [51] S. P. Adhya, C. A. Salgado, M. Spousta, and K. Tywoniuk, JHEP **07**, 150 (2020), arXiv:1911.12193 [hep-ph].
- [52] S. Schlichting and I. Soudi, Journal of High Energy Physics **2021**, 77 (2021).
- [53] P. Caucal, E. Iancu, A. H. Mueller, and G. Soyez, PoS **HardProbes2018**, 028 (2019), arXiv:1812.05393 [hep-ph].
- [54] W. Chen, S. Cao, T. Luo, L.-G. Pang, and X.-N. Wang, Phys. Lett. B **777**, 86 (2018), arXiv:1704.03648 [nucl-th].
- [55] J. Putschke *et al.*, (2019), arXiv:1903.07706 [nucl-th].
- [56] B. Schenke, C. Gale, and S. Jeon, Phys. Rev. C **80**, 054913 (2009), arXiv:0909.2037 [hep-ph].
- [57] D. Shanks, Journal of Mathematics and Physics **34**, 1 (1955), <https://onlinelibrary.wiley.com/doi/pdf/10.1002/sapm19553411>.
- [58] J. Ghiglieri, J. Hong, A. Kurkela, E. Lu, G. D. Moore, and D. Teaney, JHEP **05**, 010 (2013), arXiv:1302.5970 [hep-ph].